Report no. changed (Mar 2006): SM-327-UU

NATO UNCLASSIFIED

SACLANTCEN MEMORANDUM
serial no.: SM-327

SACLANT UNDERSEA
RESEARCH CENTRE
MEMORANDUM

TIME-EVOLUTION MODELLING OF SEAFLOOR SCATTER, PART 2: EXPERIMENTAL VERIFICATION

O. Bergem, E. Pouliquen, G. Canepa, N.G. Pace

April 1997

The SACLANT Undersea Research Centre provides the Supreme Allied Commander Atlantic (SACLANT) with scientific and technical assistance under the terms of its NATO charter, which entered into force on 1 February 1963. Without prejudice to this main task – and under the policy direction of SACLANT – the Centre also renders scientific and technical assistance to the individual NATO nations.

NATO UNCLASSIFIED

Report no. changed (Mar 2006): SM-327-UU

SACLANT Undersea Research Centre
Viale San Bartolomeo 400
19138 San Bartolomeo (SP), Italy

tel: +39-187-540.111
fax: +39-187-524.600

e-mail: library@saclantc.nato.int

NORTH ATLANTIC TREATY ORGANIZATION

Time-evolution modelling of seafloor scatter. Part II: Experimental verification

O. Bergem, E. Pouliquen,
G. Canepa, N.G. Pace

The content of this document pertains to work performed under Project 033-2 of the SACLANTCEN Programme of Work. The document has been approved for release by The Director, SACLANTCEN.

Jan L. Spoelstra
Director

intentionally blank page

Time-evolution modelling of seafloor scatter. Part II: Experimental verification

O. Bergem, E. Pouliquen, G. Canepa,
N.G. Pace

Executive Summary:

Acoustic scattering from the seafloor is a complex phenomena. A good understanding of the underlying physical process is essential to reliable remote assessment of seafloor parameters and improving MCM performance modelling.

With the recent emphasis on higher frequencies, new parameters such as seafloor roughness and sediment inhomogeneities are significant factors with concomitant effects on modelling sophistication.

This report describes a new approach for the prediction of scatter from the seafloor interface and volume in the time-domain. The report is divided into two parts. Part I describes the theoretical background of the model, part II describes the implementation and the experimental verification.

Traditionally, scattering models have focused on predicting the backscatter strength, which is basically a measurement of the energy scattered back from a unit area at a given angle. The main limitation in this approach is that all the information coming from the time-domain signal is reduced to a single number, and both phase and shape information of the original signal are lost. Here, a different approach consisting of modelling the full time-series has been chosen.

The model has been tested against simplified, but theoretically known situations and against data recorded with a parametric sonar. The results of the comparison are encouraging, and they demonstrate that the main interaction mechanisms with the seafloor are accounted for. Future work will include comparison with more data recorded from different sonar systems and with better ground truth knowledge. The use of the model for reliable remote seafloor classification will also be studied.

intentionally blank page

Time-evolution modelling of seafloor scatter. Part II: Experimental verification

O. Bergem, E. Pouliquen, G. Canepa,
N.G. Pace

Abstract: A time-evolution model of seafloor scatter is numerically implemented and experimentally verified. The model is based on expressing analytically the elementary time-backscattered response of every seafloor surface and every seafloor volume infinitesimal element. The implementation of the model is based on a statistical realization of the seabed interface and volume inhomogeneities, from which the time-series are computed by coherent summation of the scatter from small elements over the insonified area and volume. The analytical expressions and the implementation are evaluated for the image solution case, for which an almost perfect agreement is found. Examples are shown of how the beam width and seabed roughness affect the time-series return both from the surface and from the volume. The results of the model are compared with data from two different bottom types recorded with a parametric sonar. Reasonable accordance is found between the model and the data.

Keywords: ○ implementation ○ seafloor generation ○ seafloor backscattering ○ data comparison ○ model verification

Contents

List of Figures

1 Introduction

Scattering from the seafloor surface and volume are important mechanisms for numerous civilian and military reasons.

Several models have been implemented to calculate backscattering strength, e.g. [1] and [2]. In [3], analytical expressions of the time evolution approach of the seafloor scatter were presented in which sound pressure level is represented as a function of time at the receiver. The equations account for scattering from the seafloor interface and from the inhomogeneities in the volume below the interface. The water column above the seafloor interface is assumed to be homogeneous with a constant sound velocity profile.

In this paper the implementation and verification of the model are discussed. Two main issues must be considered when trying to verify the model: The validity of the theoretical basis of the model and the validity of the implementation itself. The first issue is difficult, because only for very simple cases can an analytical expression for the time domain signal be derived. One such case is the image solution, where the source and receiver are located at the same position above a flat, perfectly reflecting bottom. The verification of both the equations and the model implementations is carried out for this special case.

One form of verification is to observe the output of the model response for different input parameters. Here, the main focus is put on varying beam pattern and different seafloor roughness. Also, the effect of the horizontal correlation of the volume is studied.

In order to evaluate the model, the results are compared with data from two different bottom types. For this comparison, it is important to emphasize the experimental conditions. The model is an attempt to predict and understand the time series backscattered from different bottom types. As such, assumptions and simplifications have been incorporated in the model with respect to the physical process represented by the data recorded at sea which preclude a perfect match between the model and the data. Another complicating factor is the actual control of the acquired data. Even if great care has been taken in the acquisition process, unknown parameters will introduce errors in the data. This is especially true for the ground truth process for which only rough and limited estimates can be made.

2 Implementation

The main principles of the implementation are described in this section. The computer model is called BORIS which is an abbreviation for "BOttom Response from Inhomogeneities and Surface". A detailed specification of the implementation of BORIS is given in [4].

The following integrals from [3] are the starting points for the implementation:

$$\begin{aligned} p(\mathbf{P},t) &= p_s(\mathbf{P},t) + p_v(\mathbf{P},t) \\ &= \int_S dp_s(\mathbf{P},t) + \int_V dp_v(\mathbf{P},t) \end{aligned} \tag{1}$$

which expresses that the pressure field received at $\mathbf{P}$ from the seafloor is the sum of the elementary pressure fields integrated over the seafloor surface (S) and the seafloor volume (V). For a monostatic source and receiver with directivity pattern D_i and D_r, the seafloor surface contribution is given by

$$\begin{aligned} dp_s(\mathbf{P},t) &= \frac{\cos(\gamma(\mathbf{R}))}{2\pi \overline{c_0} R_0^2} p_0 \\ &\quad \times (D_i D_r(\mathbf{R}))\, \Re_{01}(\mathbf{R}) e^{'}(t - \frac{2R_0}{\overline{c_0}}) d\mathbf{S}_\mathbf{R} \end{aligned} \tag{2}$$

Here, $\Re_{01}$ is the local water-sediment plane wave reflection coefficient at the point $\mathbf{R}$, $\overline{c_0}$ is the average sound speed in water, $\gamma(\mathbf{R})$ is the angle between the incident direction and the vector $\mathbf{n}$ normal to the surface at $(\mathbf{R})$ and p_0 is the source level. $e^{'}(t)$ is the time derivative of the transmitted pulse $e(t)$.

The volume contribution is given by

$$
\begin{aligned}
dp_v(\mathbf{P},t) &= \frac{-n_1^2(\mathbf{R}')}{2\pi R_0^2 \overline{c_0}^2}\mu(\mathbf{R}')p_0 \\
&\times \quad D_i(\mathbf{R})D_r(\mathbf{R})\Im_{01}(\mathbf{R})\Im_{10}(\mathbf{R}) \\
&\times \quad \left(\frac{1}{\pi}\frac{\frac{\alpha R_1}{2\pi}}{(\frac{\alpha R_1}{2\pi})^2+t^2} * e''(t-2(\frac{\overline{n_1}R_1+R_0}{\overline{c_0}}))\right) \\
&\times \quad d\mathbf{V}_{\mathbf{R}}
\end{aligned} \tag{3}
$$

In this expression, $\overline{n_1}$ is the average refractive index in the first few metres of the bottom, n_1 is the local refractive index at location $\mathbf{R}'$ and R_1 is the distance of penetration into the sediment. α is the attenuation coefficient, $\Im_{01}(\mathbf{R})$ and $\Im_{10}(\mathbf{R})$ are the transmission coefficients.The double time derivative of the transmitted pulse $e(t)$ is denoted by $e''(t)$.

These equations give the sound pressure level for a given time t at position $\mathbf{P}$ by integration over the surface (S) and the volume (V). The local incident angle $\gamma(\mathbf{R})$, the local reflection coefficient $\Re_{01}(\mathbf{R})$ and the local degree of inhomogeneities in the volume $\mu(\mathbf{R}')$ are assumed to be known. Instead of using average quantities for these parameters, a different approach has been taken. Before the calculations are carried out for the integral over S, one realization of the seafloor surface and volume is calculated (see section 3). In other words, one sample from the class of seafloors having the decided statistical parameters is created and used as input to the model.

The integration is carried out by approximating the integrals with Riemann sums. The discretization is done over quadratic surface elements on the seafloor, all having the same size, independent of the incident angle. For each surface element, the local incidence angle is computed and the local reflection coefficient is calculated. The contribution from the volume is calculated for each surface element by taking the incident angle into account. This angle, which depends on the local surface slope and the reflection coefficient, gives the direction for the penetration into the volume. The total contribution from the surface and the volume element is then weighted by the actual beam pattern. This approach is followed for the whole surface (S). All calculations are done in such a way that the actual phase of the contribution to the final result is preserved.

To be able to simulate data recorded at sea, the model includes a full 3D rotation and position matrices for the source and receiver. This allows for variations of the source position, heave, pitch and roll.

It is important to notice that the model has a stochastic nature, and that the result from one run to another will be different even with the same input parameters. This is because the seafloor realization will normally change between the runs. The

model allows seafloor shape to be constant to prevent this behavior. A simplified block diagram of the model is shown in Fig. 1

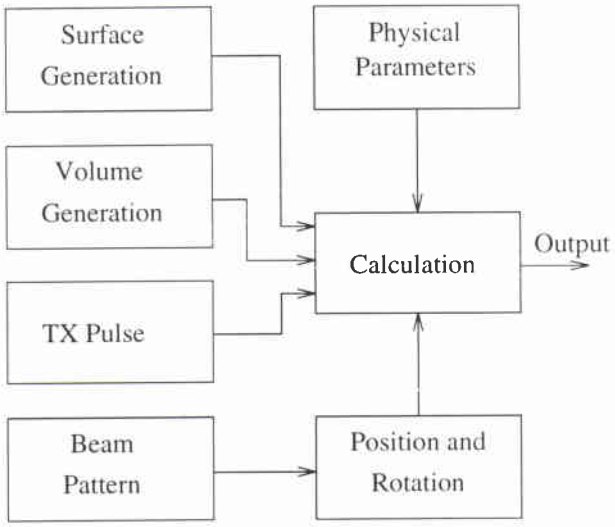

Figure 1 *Simplified box diagram of the model.*

One of the problems with the model is the storage requirement for the seafloor surface, and in particular for the seafloor volume. Depending on the resolution and the frequency, the storage required for these arrays can easily be unmanageable. In the implementation this problem is solved by dividing the seafloor into equal blocks without discontinuities in the interfaces between the blocks. Hence, only one block needs to be created and stored. Obviously this may introduce errors in the result because the surface and volume will be periodic. By keeping the block size reasonably large compared with the wave length of the signal, the effect of the error can be reduced. Care must be taken to ensure that the symmetry of the bottom is minimized with respect to the beam pattern.

3

Seafloor generation

3.1 Seafloor surface generation

Limited information on seafloor surface characteristics is available. One of the more successful methods applied to seafloor modelling is the fractal theory [6]. This theory works by generating random surface height power spectrum W_s which is converted into amplitude fields in the spatial domain using a Fourier transform.

Consider at first an isotropic heightfield h. Briggs [5] reported that the pure power law does not apply for seafloor surfaces, and a band passed power law W_s is therefore used in order to avoid an incorrect representation of the high and low frequency content:

$$\begin{aligned} W_s(\mathbf{K}) &= \eta \mathbf{K}^{-\nu} \quad if \quad K_{hp} < K < K_{lp} \\ &= 0 \quad if \quad K \leq K_{hp} \\ &= 0 \quad if \quad K \geq K_{lp} \end{aligned} \tag{4}$$

Here $\mathbf{K}$ is a two-dimensional wave vector with a magnitude equal to the wave number K. The high pass cutoff wave number is K_{hp} , the low pass cutoff wave number is K_{lp}, and ν is related to the fractal dimension and accounts for the decay of the power spectrum. η is the normalization factor so that locally:

$$\int_{-\infty}^{\infty} \int_{-\infty}^{\infty} W_s(\mathbf{K}) d^2\boldsymbol{k} = \sigma_h^2 \tag{5}$$

Here, σ_h is the rms height of the isotropic generated height field $h(\mathbf{r})$ assuming that this process is locally stationary.

The high and low pass filtering of the power spectrum has a physical meaning. By removing the low frequency content of the spectrum, the large scale oscillations are canceled which is sensible if one consider that sedimentary regions are more often flat than undulating. The high frequency content of the spectrum is related to the shear strength in the sediment. According to Briggs [5], the values of the slope of the

roughness power spectrum vary with sediment type rather than with the presence or the absence of anisotropic roughness. On the contrary, bioturbation seems to strongly modify the statistics of the surface.

Observation of the seafloor shows that sandy seafloors contain anisotropic components. In order to take this phenomena into account, a ripple heightfield $g(\mathbf{r})$ can be added to the previous heightfield $h(\mathbf{r})$ in order to construct the total heightfield $z(\mathbf{r})$. The proposed power spectrum W_g for this heightfield $g(\mathbf{r})$ has the following form:

$$W_r(\mathbf{K}) = \frac{\sigma_r^2}{\sqrt{2\pi}K_\sigma} e^{-\frac{(|\mathbf{K}-\mathbf{K_c}|)^2}{2K_\sigma^2}} \tag{6}$$

In this power spectrum, K_c defines the central wave number vector of the ripples (it sets the direction of this field and its average wavelength). K_σ defines the dispersion (or the rms distribution) of these ripples in the spectrum itself and σ_r is the rms roughness of the ripple field. Then, if a seafloor surface is a combination of a filtered power law derived heightfield and of a ripple heightfield, one has:

$$z(\mathbf{r}) = h(\mathbf{r}) + g(\mathbf{r}) \tag{7}$$

$$\sigma_z^2 = \sigma_h^2 + \sigma_g^2 \tag{8}$$

To illustrate the surface generation, two seafloor realizations are presented in Fig. 2 and Fig. 3 using image rendering techniques. The scenes are illuminated by a source light located 1 metre above the average height of the seafloor. The first image shows a muddy sediment with high bioturbation, while the second shows a sandy bottom with ripples.

3.2 Seafloor volume generation

Marine sediments are inhomogeneous, which means that there are spatial fluctations in the sound speed, density, attenuation, porosity or grain size. These fluctuations have important consequences for the geo-acoustical properties of the seafloor, but unfortunately these variations are particularly difficult to measure to the required spatial resolution. The use of core sampling is not adequate because it only gives a sparse and vertical information on the actual 3D random inhomogeneity field. In order to obtain more information in the horizontal direction, core samplings should be multiplied but this is technically difficult. Measurement of volume inhomogeneities

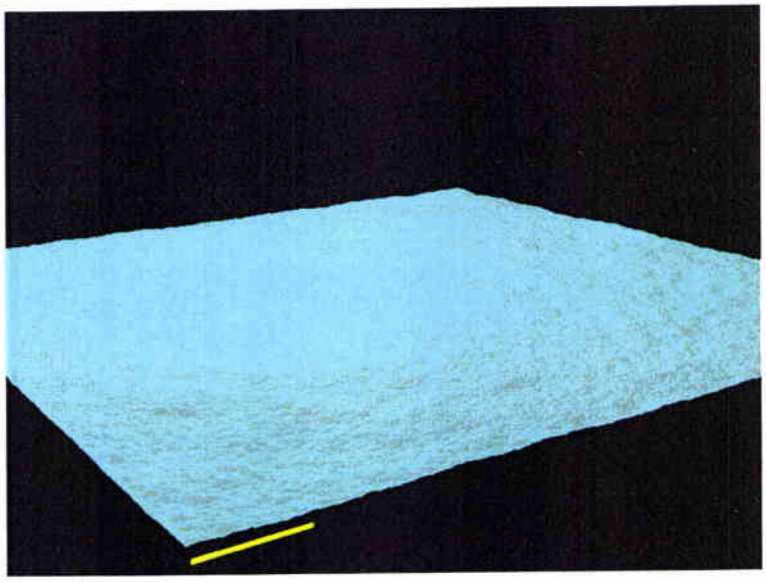

Figure 2 $10m \times 10m^2$ *generated surface of a muddy seafloor with high bioturbation:* $\sigma_z = 3cm$, $\nu = 3$, $K_{hp} = 1rad/m$, $K_{lp} = 200rad/m$. *1 metre on the images is represented by the white bars.*

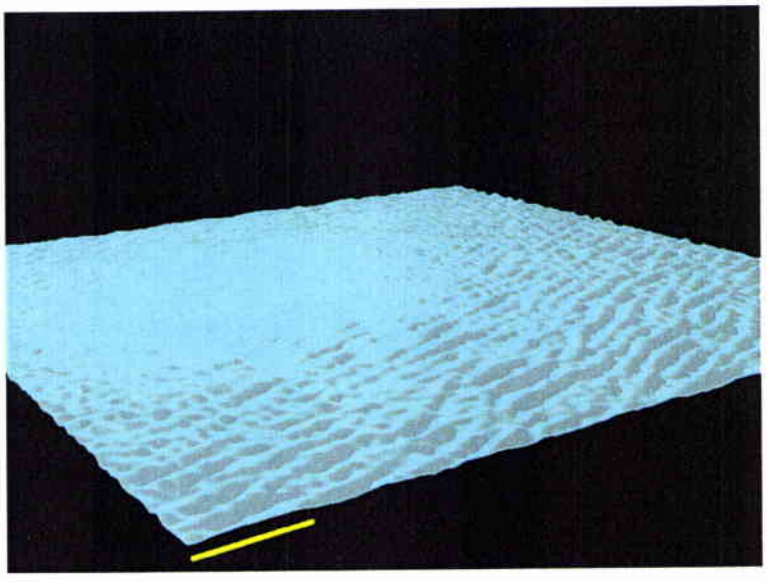

Figure 3 $10m \times 10m$ *generated surface of a sandy seafloor with presence of ripples in a* $20°$ *direction versus the left border of the image:* $\sigma_z = 3cm$, $\sigma_h = 0.0212cm$, $\sigma_g = 0.0212cm$, $\nu = 2$, $K_{hp} = 1rad/m$, $K_{lp} = 40rad/m$. *1 metre on the images is represented by the white bars.*

has been neglected until recently because volume scattering in high frequency acoustics has been considered as a secondary physical phenomena. The physical entity for characterizing seafloor volume inhomogeneities is usually the 3D power spectrum of correlation W_v which is the Fourier transform of the 3D correlation function B_v accounting for sound speed and density variations at mean values. However, knowledge of the correlation function is weak, and there is little evidence for or against the selection of any particular function. For the BORIS model an exponential correlation function has been used:

$$B_v(\mathbf{R}') = \mu^2(\mathbf{R}')exp\left(-\frac{|z_1|}{l_v} - \frac{r}{l_h}\right) \tag{9}$$

Here l_v and l_h are respectively named vertical correlation length and horizontal correlation length. The Fourier transform of the chosen correlation function can be expressed analytically:

$$W_v(\mathbf{K}) = \mu^2(\mathbf{R}')\left(\frac{l_v}{\pi(1+K_{z_1}^2 l_v^2)}\frac{l_h^2}{2\pi(1+K_r^2 l_h^2)^{3/2}}\right) \tag{10}$$

where $\mathbf{R}' = \mathbf{z_1} + \mathbf{r}$ and $\mathbf{K} = \mathbf{K_{z_1}} + \mathbf{K_r}$. As far as the choice of l_v and l_h, it is reasonable to assume that sound speed and density vary more in the vertical direction than in the horizontal direction. Gensane [7] finds that on average l_h is approximately 5 times l_v. This implies that even in surficial sediments, the idea of layering persists, or in other words, sediment properties are more stationary in the horizontal direction than in the vertical one. This is valid for slightly perturbated sediments and does not apply to highly bioturbated sediments where isotropy can be assumed ($l_v = l_h$).

4

The image solution and reflection loss

The simplest test of the model is a comparison with the image solution, which corresponds to the imaginary image of the source on the opposite side of a perfectly reflecting, flat surface. For this simple case, an analytical expression can be obtained. For simplicity, assume that $p_0 = 1$. With an omnidirectional receiver and transmitter and a flat, perfectly reflecting bottom, Eq. (2) becomes

$$dp_s(\mathbf{P},t) = -\frac{\cos(\theta)}{2\pi\overline{c_0}R_0^2}e^{'}(t-\frac{2R_0}{\overline{c_0}})d\mathbf{S_R} \tag{11}$$

where θ is the incident angle. Looking at the full integral with a source at height H above the bottom ($\cos\theta = H/R_0$), one obtains

$$p_s(\mathbf{P},t) = -\int_{(S)}\frac{\cos(\theta)}{2\pi\overline{c_0}R_0^2}e^{'}(t-\frac{2R_0}{\overline{c_0}})d\mathbf{S_R} \tag{12}$$

$$= \int_{(S)}\frac{H}{2\pi\overline{c_0}R_0^3}e^{'}(t-\frac{2R_0}{\overline{c_0}})d\mathbf{S_R} \tag{13}$$

Using polar coordinates, the above equation can be written as

$$p_s(\mathbf{P},t) = -\int_0^\infty\int_0^{2\pi}\frac{H}{2\pi\overline{c_0}R_0^3}e^{'}(t-\frac{2R_0}{\overline{c_0}})rd\theta dr \tag{14}$$

$$= -\frac{H}{\overline{c_0}}\int_0^\infty\frac{e^{'}(t-\frac{2R_0}{\overline{c_0}})}{R_0^3}rdr \tag{15}$$

Using the fact that

$$R_0^2 = r^2 + H^2 \tag{16}$$

one can write

$$\frac{de}{dt} = -\frac{c_0\sqrt{r^2+H^2}}{2r}\frac{de}{dr} \tag{17}$$

Using Eq. (16) and Eq. (17), Eq. (15) can be written as

$$p_s(\mathbf{P},t) = \frac{H}{2}\int_0^\infty \frac{\frac{de}{dr}}{r^2+H^2}dr \tag{18}$$

Integrating by parts one obtains

$$p_s(\mathbf{P},t) = \left.\frac{He(t-\frac{2\sqrt{r^2+H^2}}{\overline{c_0}})}{2(r^2+H^2)}\right|_{r=0}^{\infty} + \int_0^\infty \frac{He(t-\frac{\sqrt{r^2+H^2}}{\overline{c_0}})r}{(r^2+H^2)^2}dr \tag{19}$$

The first part equals

$$-\frac{e(t-\frac{2H}{\overline{c_0}})}{2H} \tag{20}$$

which is the image solution expected from a flat, perfectly reflecting surface at a distance H. The contribution of the last integral will depend on the transmitted pulse as well as the height H and the sound speed $\overline{c_0}$. If the pulse has a dominant frequency f_0 the last term will be small compared to the image solution if $\lambda_0 << H$, which reflects the far field assumption made for the Kirchhoff approximation.

In Fig. 4 the result of a run from the model is plotted with the theoretical solution for a 5 kHz Ricker pulse. The source and receiver are situated 10 m above a flat, infinitely hard bottom. The sampling rate of the signal was 1MHz and the surface resolution 0.005 m. These values were selected in order to minimize numerical inaccuracies. There is no discernible difference between the two pulses for this special case. As the bottom is perfectly flat and homogeneous, the seafloor realization will be unique, and no variations will be seen in the model between different runs.

Another simple test of the model can be carried out by comparing the model return with the Rayleigh reflection coefficient given by

$$\Re = \frac{(Z_1 - Z_0)}{Z_1 + Z_0} \tag{21}$$

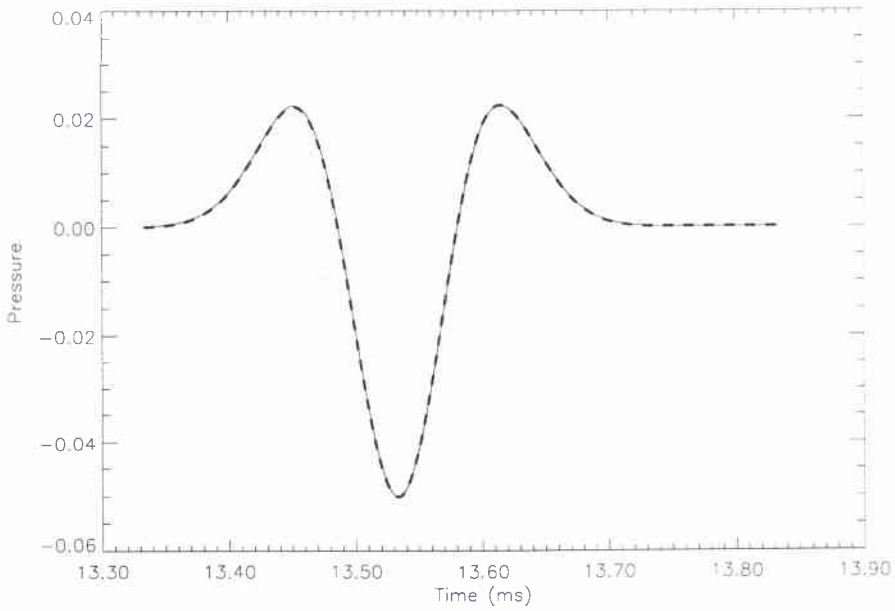

Figure 4 *Comparison between the theoretical solution (solid) and the model (dashed) for a flat, infinitely hard bottom. The pulse is a Ricker pulse and the source-receiver location is 10 m above the bottom.*

where Z_1 and Z_0 are the acoustic impedances of the seafloor and the water column respectively. This expression is valid for plane waves at normal incidence. If the bottom is flat and homogeneous, the source is located far from the seafloor (in term of wave lengths) and the beam width is wide, the reflection coefficient for a spherical wave can be approximated by

$$\Re \approx \frac{\int_{\frac{2H}{C_0}}^{\frac{2H}{C_0}+l} p_r(t)^2 dt}{2H \int_0^l p_t(t)^2 dt} \tag{22}$$

Here $p_r(t)$ and $p_t(t)$ are the reflected and transmitted pressures respectively and l the length of the transmitted pulse.

The model was run using the previous Ricker pulse for three different bottom types: sand, silt and clay. The reflection coefficients were calculated using Eq. (22), and the results are shown in Table 1. The change in impedance is easily seen in the results computed by the model; for the softer bottoms the energy penetrates into the sediment instead of being reflected.

The values in Table 1 agree with the reflection coefficients given by Eq. (21) to the

third decimal.

Table 1 *Calculated reflection coefficient using Eq. (22) for a flat surface.*

Bottom Type	Sound speed (m/s)	Density (g/cm^3)	$\Re$
Sand	1720	1.9	0.371
Silt	1610	1.7	0.292
Clay	1510	1.5	0.203

5 Model simulations

5.1 Seafloor surface contribution

The first simulation examines the effect of the roughness of a sandy seafloor surface on the received pulse. The volume contribution is set to zero to emphasize the effect on the surface roughness. The beam is omnidirectional, and the transducer is situated 10 metres above the bottom. The transmitted pulse is a Ricker pulse centered at 5 kHz. The value of all parameters used is shown in column 2 (Surface runs) of Table 2. Figure 5 shows the result of the simulation.

Table 2 *Model parameter settings.*

Parameters	Surface runs	Volume runs	Sand	Clay
Surface increment dp_s (m)	0.03	0.03	0.03	0.03
Volume increment dp_v (m)	-	0.03	0.03	0.03
Depth H (m)	10.0	10.0	14.5	11.9
Sound speed, c_1 (m/s)	1720	1510	1270	1475
Density ρ_1 (g/cm^3)	1.90	1.50	1.90	1.55
Surf. rms rough. σ_h (m)	0.0 (Varying)	0.02	0.01	0.01
Surf. pow. e-p. ν	2.0	2.0	2.0	2.0
LP cutoff K_{lp} (rad/m)	50	50	50	35
HP cutoff K_{hp} (rad/m)	1	1	1	1
Volume inhomog. μ	-	0.02	0.02	0.02
Volume Hor. Cor. l_h (m)	-	1.0 (Varying)	0.5	0.4
Volume Ver. Cor. l_v (m)	-	0.05 (Varying)	0.02	0.01
Attenuation β (dB/m)	-	0.5 (Varying)	0.9	0.5

For a flat bottom ($\sigma_z = 0.0cm$) the returned signal shape closely resembles the transmitted signal with the amplitude reduced by the transmission loss ($2H$) and the reflection loss. With an rms roughness of only 0.5 cm, the effect of returns from off normal incidence is clearly visible. As the seafloor was unchanged during this simulation, the surface has the same shape, and the same features seem to become increasingly apparent as the roughness is increased. Looking at the small peak at 15.6 ms, this is not always the case, as this peak decreases for $\sigma_z = 6.0$ cm. At 5-6 cm rms roughness the coherent reflection has almost disappeared, and the incoherent scattering from off normal incidence dominate the signal.

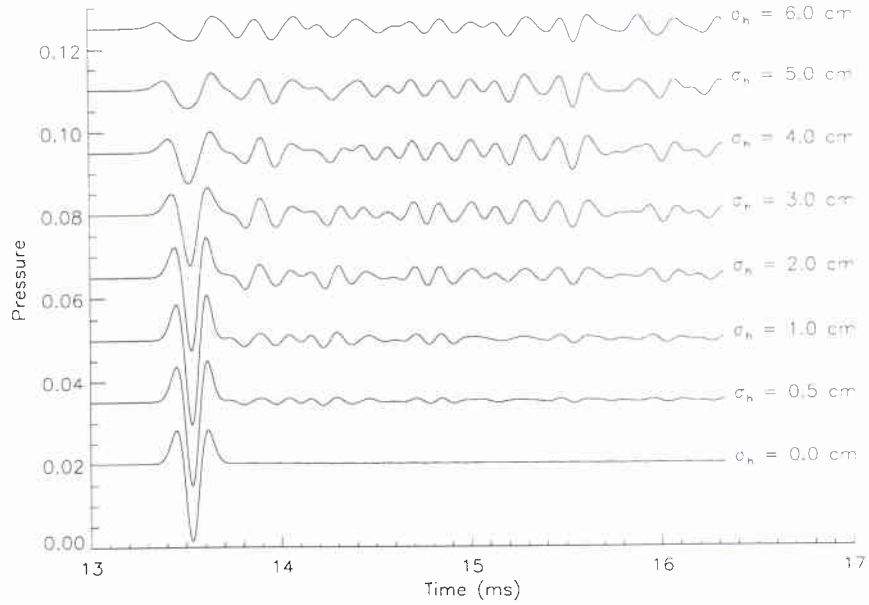

Figure 5 *Returned signal from the seafloor surface as function of the rms roughness for an omnidirectional beam.*

It is interesting to examine the influence of the beam pattern on the reflected pulse. Looking at Eq. (2), the return from the surface consists of a time shifted and amplitude weighted sum of the derivatives of the pulse. The effect of this can be observed in Fig. 6. Here, the model has been run over a flat, sandy surface with varying beam patterns. For the purpose of this illustration, the beam patterns of amplitudes versus angles have a Gaussian shape, and the angles in the figure are the half beam width measured at e^{-1}. The other parameters for the run are the same as in column 2 (Surface runs) in Table 2. For wide angles, the returned pulse is close to the expected image solution as seen previously. When the beam is narrowed, the size of the integration surface S is reduced, and the pulse starts to change the shape and amplitude. This effect is due to the fact that any directional beam requires more than one point source to be formed. Hence, the total field can be viewed as a coherent summation of the field from imaginary sources, and the returned pulse will consist of a sum of pulses shifted in time (Fig. 7). If the pulse is not a CW, the shape will then be changed with respect to the transmitted pulse from each source. This effect is important when estimating the reflection coefficient or when looking at the shape of the reflected pulse for seafloor classification.

A combination of the two previous runs is presented in Fig. 8. For this run, the surface roughness is 3.0 cm and the beam width is varying. The other parameters are the same as before. With a beam width of 30° the result looks similar to the

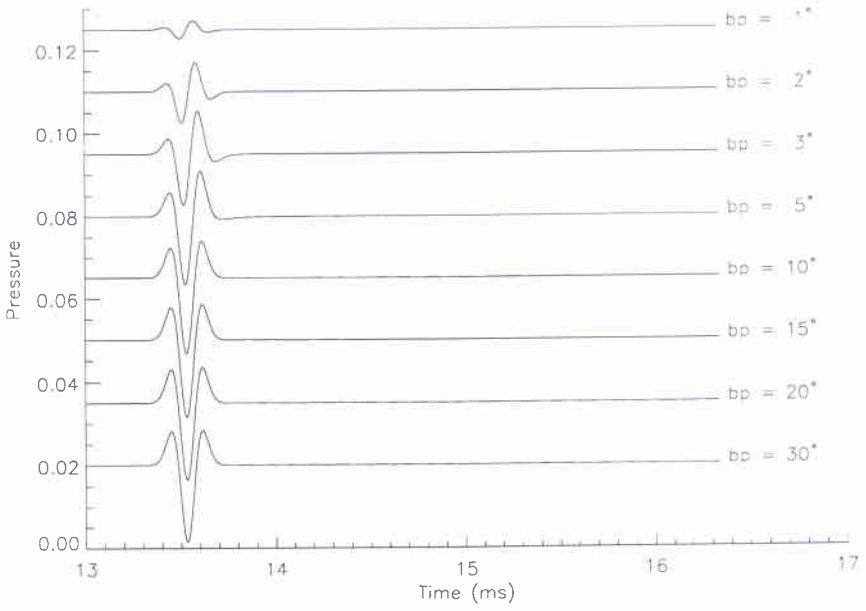

Figure 6 *Returned signal from the seafloor surface as function of the beam pattern for a flat bottom.*

omnidirectional beam in Fig. 5, except that the tail of the signal has less energy due to the reduced beam width. As the beam narrows, the scattering from the side of the beam is reduced, and consequently less energy is seen in the tail. The effect of the roughness is however not removed. Looking at the amplitude of the 3° beams in Fig. 6 and Fig. 8, one can see that even though the shape is similar, the amplitude of the coherent reflection in Fig. 8 is reduced by a factor of almost 2 due to the roughness.

5.2 Volume contributions

Volume scattering contributes to the total scatter at a level which is directly proportional to the degree of inhomogeneities $\mu^2(\mathbf{R}')$ (Eq. (3)). The result is a weighted and time shifted combination of the second derivative of the transmitted pulse, convolved with the frequency dependent attenuation.

As with the surface contribution, a few test cases have been selected to illustrate the results from the model. The model parameters for the runs are shown in column 3 (Volume runs) in Table 2. The bottom is composed of silt, the depth is 10 m, and the beam width is 30°. The same realization of the seafloor volume and surface are used in each run in order to allow comparison of results. The first case is presented

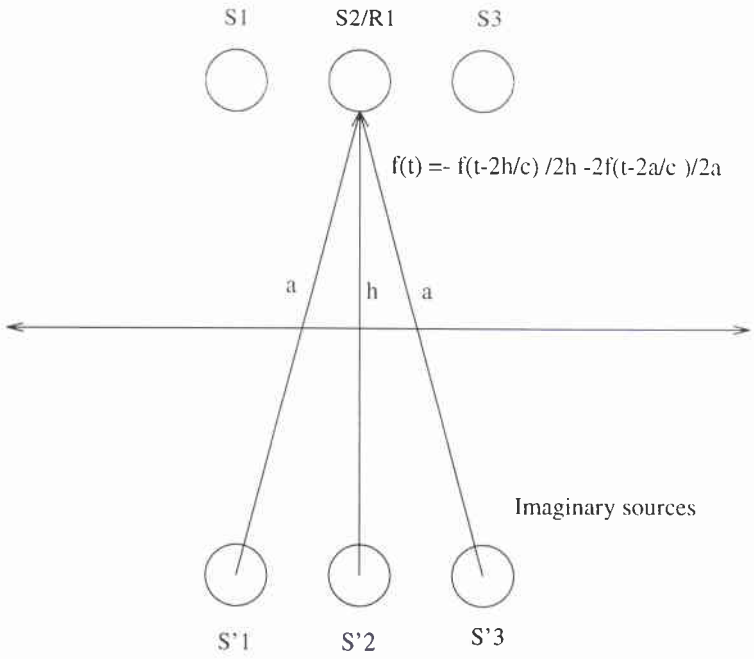

Figure 7 *The pulse received at R1 are the coherent summation of the pulses from the imaginary sources S'1-S'3*

in Fig. 9, where the return from the volume is shown as a function of the attenuation in the sediment. Looking carefully at the last parts of the signals, one can see that the higher frequencies are more attenuated than the lower (e.g. the knee at 16.3 ms). This is a consequence of using Eq. (3) in the model which includes the convolution process and effectively works as a low pass filter on the returned scatter.

The beam pattern is also important when looking at the volume return. Figure 10 shows examples of the volume return for different beam patterns.

The results are interesting, because they show that the scatter from the outer part of the beam contributes extensively to the final result. Hence, a narrow beam does not only reduce the surface scatter, but also the volume contribution. The same experiment is repeated in Fig. 11, but the horizontal correlation of the volume is reduced from 1.0 m to 0.05 m. It should be noted that this implies a change in the realization of the volume, which means that the result can not be directly compared to the first. It is seen that the general level of the volume contribution decreases, and the effect of the beam width is even more important. This result is expected, because the lower correlation means increased randomness in the volume. With no horizontal or vertical correlation at all, the total contribution from the volume should be zero.

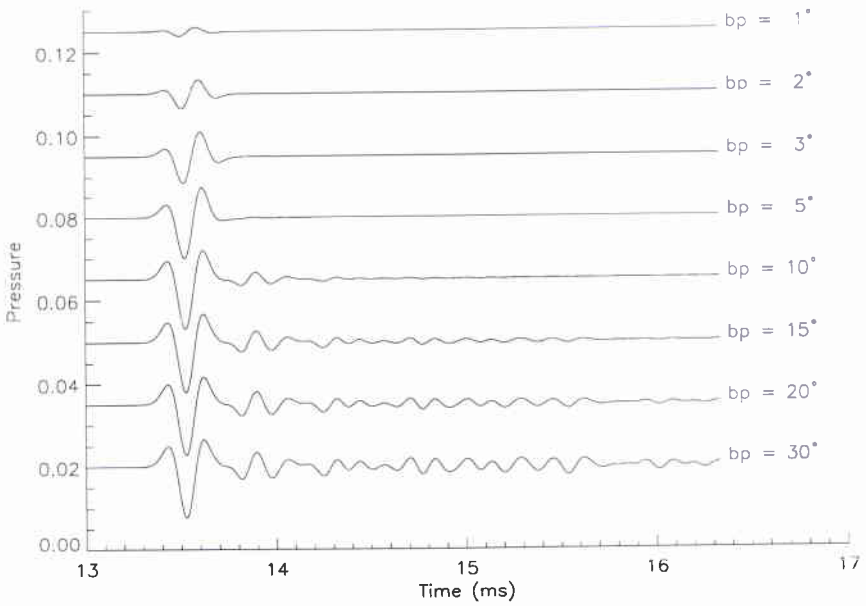

Figure 8 *Returned signal from the seafloor surface as function of the beam pattern. Surface rms roughness 3.0 cm.*

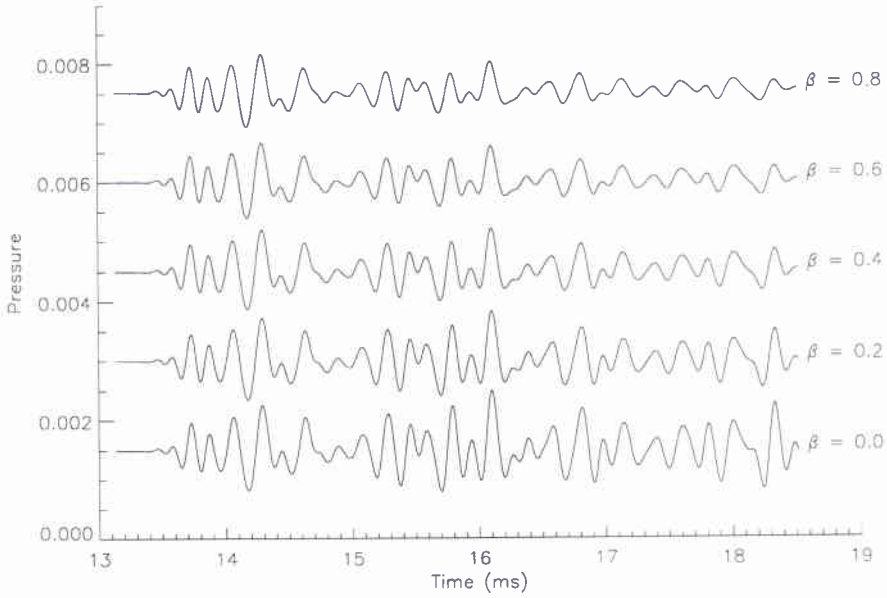

Figure 9 *Returned signal from the seafloor volume as function of the sediment attenuation β.*

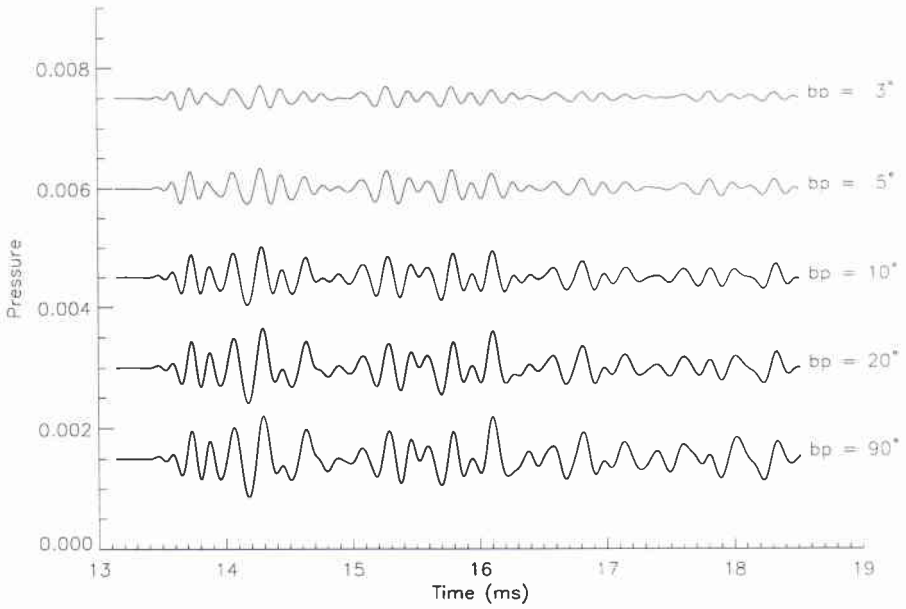

Figure 10 *Returned signal from the seafloor volume as function of the beam width. Horizontal volume correlation 1.0 m.*

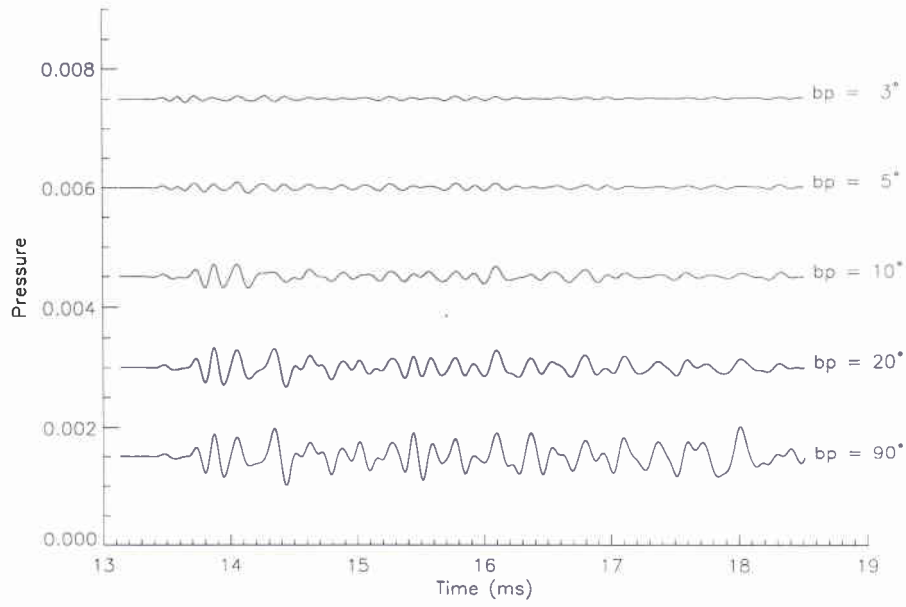

Figure 11 *Returned signal from the seafloor volume as function of the beam width. Horizontal volume correlation 0.05 m.*

6

Comparison with data

The Simrad TOPAS 040 parametric system has been used to acquire data from different bottom types in the Golf of La Spezia, Italy. The parametric sonar has a primary frequency centered at 40 kHz, the secondary frequencies are in the 1-12 kHz range. The sonar was calibrated and mounted in a free floating buoy during the experiments [8]. A Ricker pulse, similar to the one used in the previous simulations, was input to the model. The centre frequency of the pulse is around 8 kHz and the source level around 206 dB ref 1μPa. The pulse and the beam pattern used as input to the model are based on data recorded during the calibration. A filter was used during the acquisition of the data, and in order to visually compare the results, the same filter has been applied to the time series from the model. The filter includes the effects of the reflections in the buoy and the band pass filter of the recorder. The transmitted pulse together with the effect of the filter is shown in Fig. 12.

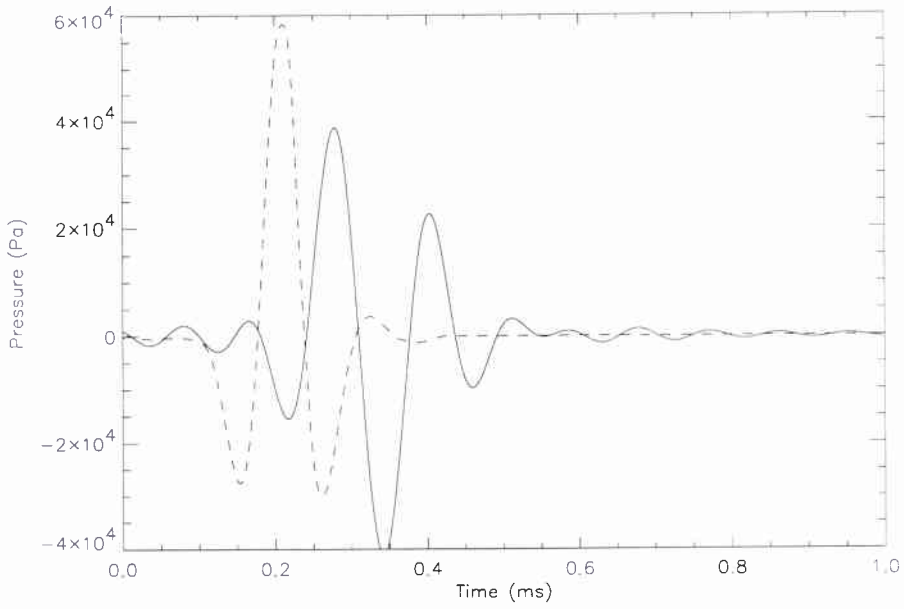

Figure 12 *The transmitted pulse (dashed) and the resulting pulse (solid) after application of the filter which accounts for the effects of the recording system.*

The only directly measurable parameters from the ground truth process are the

sound speed and density, the roughness parameters from the surface are based on visual estimates from under water photographs. The volume parameters are based on sound velocity measurements in the cores. However, the measuring technique probably underestimates the variation due to insufficient resolution in the probes.

6.1 Compacted sand

The Tellaro site is characterized by flat, compacted sand close to the shore with a transition to silt as one moves away from the coast. The data presented here were acquired close to the shore. A traditional seismic profile shows that there are no major sub layers up to 9 ms after the interface, but a relatively high scattering density is seen from the upper part of the sediment. Photographs show very low roughness and some biological activity. Several cores have been taken from the site, but as the corer only penetrates a few decimetres into the sediment the volume inhomogeneity profile can only be roughly estimated in the upper part. The parameters used as input to the model are shown in column 4 (Sand) in Table 2.

In Fig. 13, five pings of data recorded at the site are shown. They are all taken with the ship anchored at the same position, but with small differences in heading and position. The strong seafloor reflection dominates the signal, and very little energy is present in the tail.

Figure 14 shows the results of five runs from the BORIS model. The model was run with the same parameters each time, but the realizations of the surface and the volume were different. The correspondence between the signals from the data and the model is good, and the predicted amplitude is very close to the measured values. The runtime for five simulations was of the order of one minute on a workstation.

6.2 Clay

The bottom of the bay of Portovenere consists of a relatively homogeneous layer of clay, but to the south side of the bay, more scattering from the volume is observed. The data presented here are recorded in the latter part. The underwater camera shows some biological activity, but generally the surface is relatively flat. The parameters which have been used are shown in column 5 (Clay) of Table 2. The data (Fig. 15) show a clear indication of sub layers. This can be observed at all pings around 17 ms. The amplitude is lower than for the sandy site, and the volume return is stronger. The results from five runs of the model are shown in Fig. 16. Again, the variation between the pings is higher than in the data, and the volume return appears at different places because no distinct sub layers have been input to the model. The amplitude of the signals is close to the recorded amplitude.

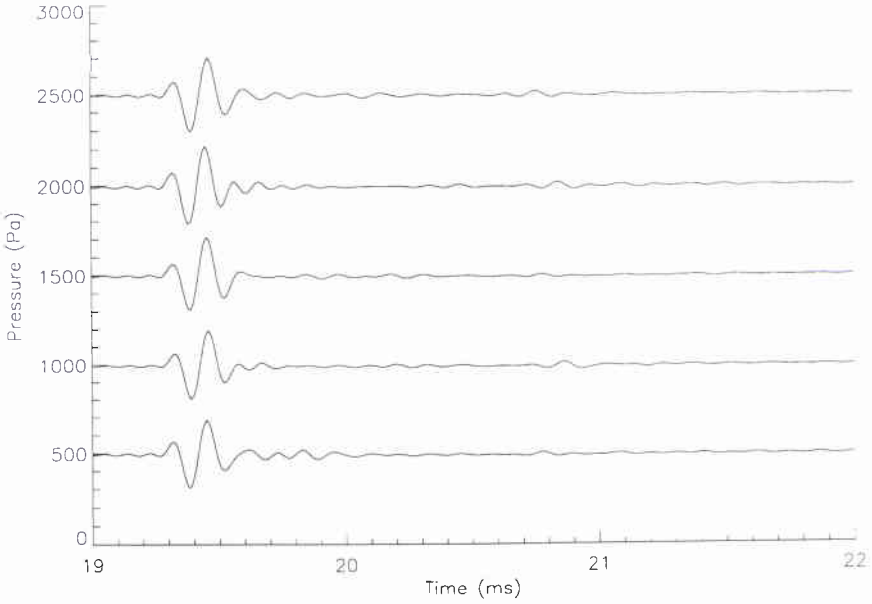

Figure 13 *Recorded data. Bottom: Compacted sand.*

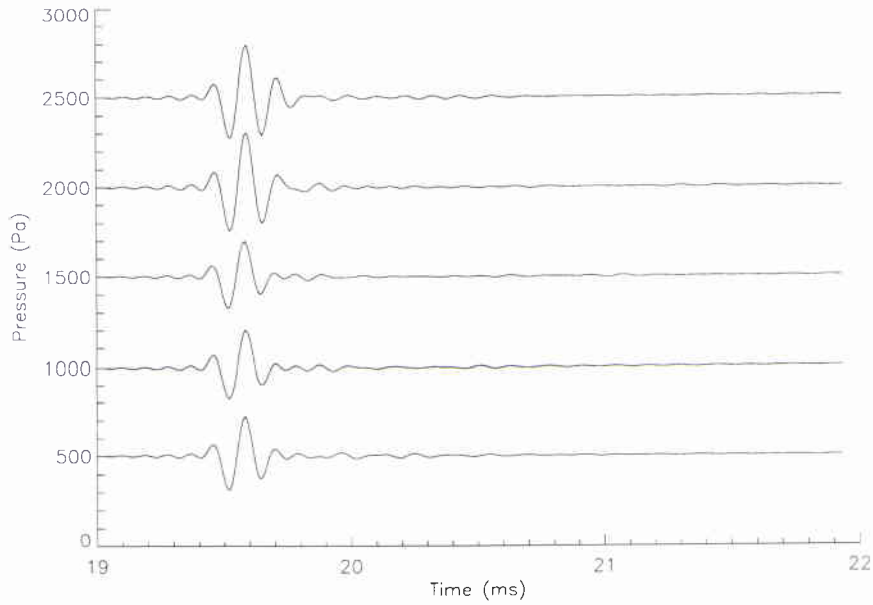

Figure 14 *BORIS simulated data. Bottom: Compacted sand.*

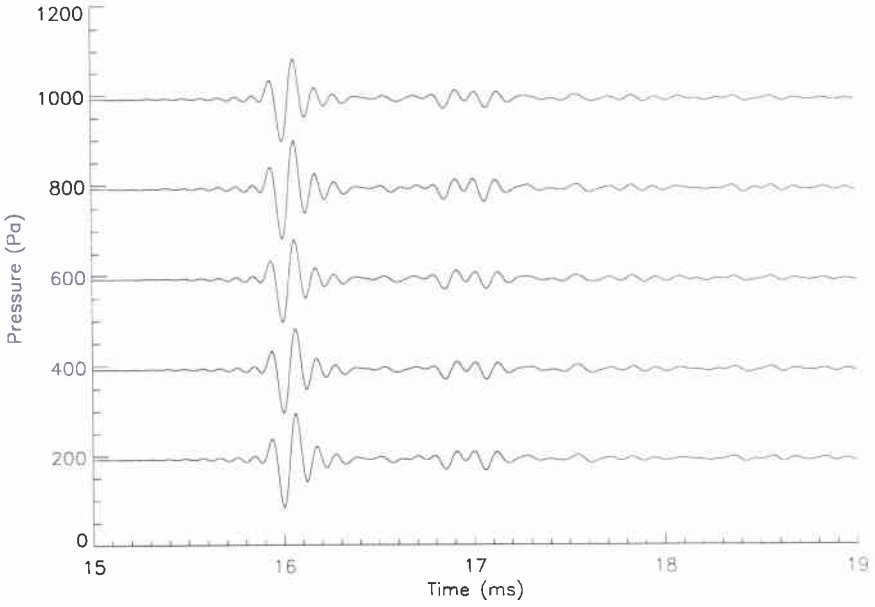

Figure 15 *Recorded data. Bottom: Clay. A layer is clearly seen at 17 ms.*

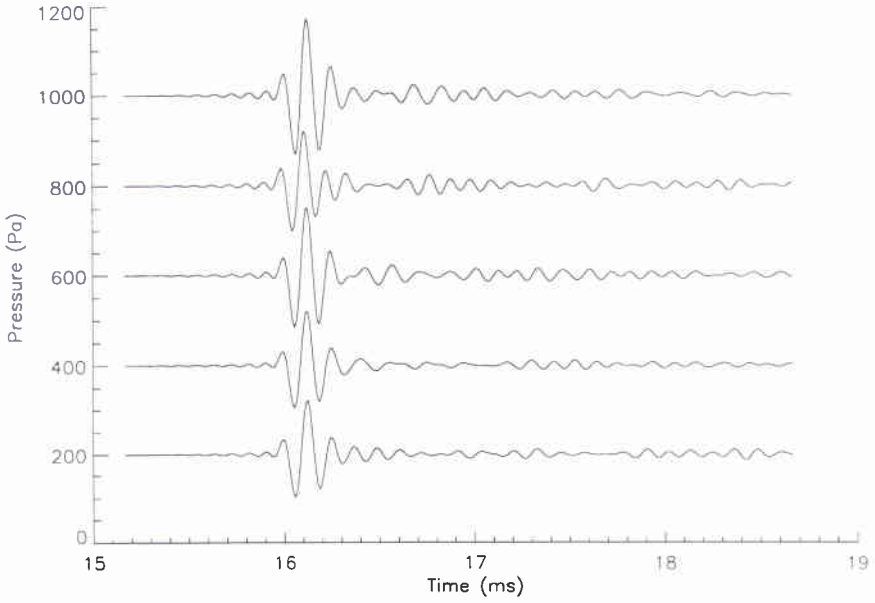

Figure 16 *BORIS simulated data. Bottom: Clay. No specific layer is seen due to the different realizations of the volume.*

To illustrate the contribution from the volume and surface more clearly, the simulated responses are plotted separately in Fig. 17. The solid line shows the volume contribution and the dashed line shows the surface contribution. The coherent sum of these two contributions is the same as the lowest ping in Fig. 16. It is interesting to note that in this case the maximum amplitude of the surface response is about five times stronger than for the volume.

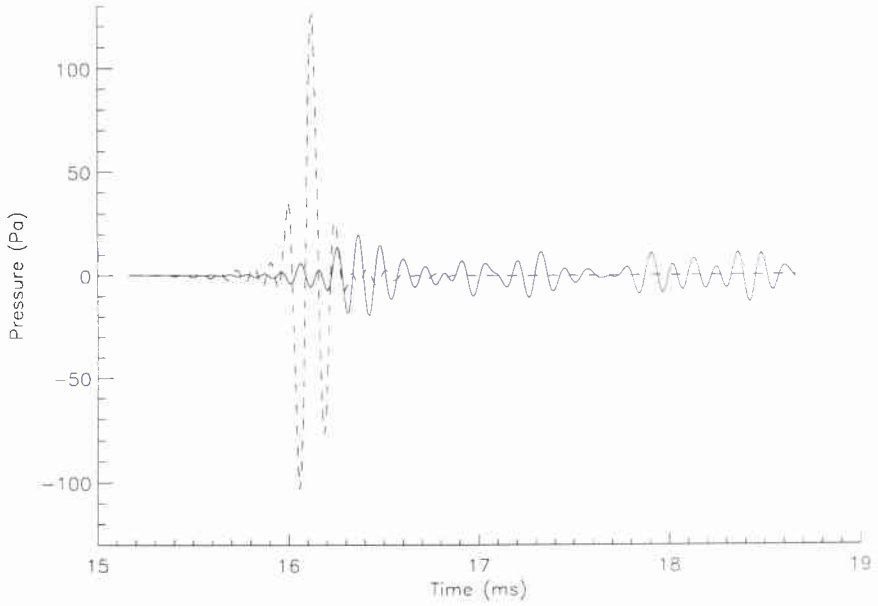

Figure 17 *Simulated surface and volume contributions. Bottom: Clay. The solid line shows the volume contribution, the dashed line shows the surface contribution.*

6.3 Comments

The model seems to include the main physical mechanisms of an interaction of a short pulse with the seafloor. The shape and the amplitude of the times series predicted by the model are close to the data recorded at sea. It seems that the volume contribution from the model is slightly too low for both cases, but it is difficult to judge whether this is due to problems with the ground truth procedure or the model itself.

A more general problem encountered is the effect of the bottom generation. The data are recorded with slight changes in position and heading over the same bottom, while the model is run with a different realization of the bottom for each run. The result is, that the change from one run to the other is higher for the model than the change in the recorded data between two pings. An alternative approach would be to

use one bottom realization for the model, but move the source as in the experiment. This may or may not give a better result, depending on the similarity between the real bottom and the generated bottom. Essentially, the problem arises from the fact that a statistical description can only give at best a statistically satisfactory result. A one to one correspondence between snapshot data and model can not be expected.

7 Summary

In this paper we have implemented the time-evolution model for seafloor scatter presented in [3]. The model calculates the time series return from the seafloor based on scattering from the interface and from inhomogeneities in the volume. The interface and volume are described with statistical parameters, and for each run the model creates one realization of each of these and calculates the return. For the surface generation Fourier synthesis is used to produce the height field, while for the volume part an exponential correlation function has been used to generate variations in the sound speed and density. The final return is a summation of contributions from elementary surface- and volume elements based on analytical expressions.

The model was run and results given for different input parameters. The effect of interface roughness was illustrated, and it was shown how different beam patterns affect the time domain signal. Examples of the volume contributions were also shown. Comparison with data recorded by a calibrated parametric array was carried out for two different bottom types consisting of compacted sand and clay. Good agreement was found between the data and the model both with respect to the shape and the amplitude of the signal. A problem with the comparison was that some of the input parameters to the model were difficult to estimate from the ground truth data. This was especially apparent for the volume inhomogeneity distribution.

The model appears to predict well the scattering from the seafloor interface and volume, and it would appear to be a valuable tool for studying the geometric and environmental effects on the time domain signals. Further work is needed in order to evaluate the model against different sonar systems and frequencies.

Acknowledgments

This work is partially supported by EU, under the MAST-III initiative, project "ISACS", contract no. MAS3-045.

References

[1] D. R. Jackson, D. P. Winnebrenner, A. Ishimaru. Application of the composite roughness model to high-frequency bottom backscattering. *Journal of the acoustical society of America*, **79**, 1410-1422, (1986).

[2] F. A. Boyle and N. P. Chotiros. A model for acoustic backscatter from muddy sediments. *Journal of the acoustical society of America*, **98**, 525-530, (1995).

[3] E. Pouliquen, O. Bergem, N. G. Pace. Time-evolution modelling of seafloor scatter, Part1: Theory. SACLANTCEN SM-328. La Spezia, Italy, SACLANT Undersea Research Centre, (1997).

[4] G. Canepa, O. Bergem, E. Pouliquen. The implementation of BORIS-3D: BOttom Response from Inhomogeneities and Surface, Version 1.0. SACLANTCEN M-125. La Spezia, Italy, SACLANT Undersea Research Centre, (1997).

[5] K. B. Briggs. Microtopographical roughness of shallow-water continental shelves. *IEEE Journal of Oceanic Engineering*, **14**, 360-367, (1989).

[6] M. F. Barnsley, R. L. Devaney, B. B. Mandelbrot, H. O. Peitgen, D. Saupe and R. F. Voss. The science of fractal images, (Springer-Verlag 1988).

[7] M. Gensane. Sea-bottom reverberation: the role of volume inhomogeneities of the sediment. In Ocean Reverberation, edited by D. D. Ellis, J. R. Preston, H. G. Urban, 59-64. (Kluwer 1993).

[8] O. Bergem & N.G. Pace. Installation and calibration of a parametric array for shallow water backscatter measurements. In Proc. Oceans 96, Fort Lauderdale, (1996).

Report no. changed (Mar 2006): SM-327-UU

Document Data Sheet

NATO UNCLASSIFIED

Security Classification		Project No.
NATO UNCLASSIFIED		033-2
Document Serial No.	**Date of Issue**	**Total Pages**
SM-327	April 1997	33 pp.

Author(s)

Bergem, O., Pouliquen, E., Canepa, G., Pace, N.G.

Title

Time-evolution modelling of seafloor scatter, Part II: Experimental verification

Abstract

A time-evolution model of seafloor scatter is numerically implemented and experimentally verified. The model is based on expressing analytically the elementary time-backscattered response of every seafloor surface and every seafloor volume infinitesimal element. The implementation of the model is based on a statistical realization of the seabed interface and volume iinhomogeneities, from which the time-series are computed by coherent summation of the scatter from small elements over the insonified area and volume. The analytical expressions and the implementation are evaluated for the image solution case, for which an almost perfect agreement is found. Examples are shown of how the beam width and seabed roughness affect the time-series return both from the surface and from the volume. The results of the model are compared with data from two different bottom types recorded with a parametric sonar. Reasonable accordance is found between the model and the data.

Keywords

implementation – seafloor generation – seafloor backscattering – data comparison – model verification

Issuing Organization

North Atlantic Treaty Organization
SACLANT Undersea Research Centre
Viale San Bartolomeo 400, 19138 La Spezia,
Italy

*[From N. America: SACLANTCEN
(New York) APO AE 09613]*

Tel: +39 (0)187 540 111
Fax:+39 (0)187 524 600

E-mail: library@saclantc.nato.int

NATO UNCLASSIFIED

Initial Distribution for SM-327

SCNR for SACLANTCEN		*National Liaison Officers*	
SCNR Belgium	1	NLO Canada	1
SCNR Canada	1	NLO Denmark	1
SCNR Denmark	1	NLO Germany	1
SCNR Germany	1	NLO Italy	2
SCNR Greece	2	NLO Netherlands	1
SCNR Italy	1	NLO UK	3
SCNR Netherlands	1	NLO US	4
SCNR Norway	1		
SCNR Portugal	1		
SCNR Spain	1		
SCNR Turkey	1		
SCNR UK	1		
SCNR US	2		
French Delegate	1		
SECGEN Rep. SCNR	1	Total external distribution	34
NAMILCOM Rep. SCNR	1	SACLANTCEN Library	26
SACLANT	3	Total number of copies	**60**